Accepted for publication in *Journal of Geophysical Research.*

Vortexwide Denitrification of the Arctic Polar Stratosphere in Winter 1999/2000 determined by Remote Observations

Armin Kleinböhl, Holger Bremer, Miriam von König, Harry Küllmann, and Klaus F. Künzi
Institute of Environmental Physics, University of Bremen, Bremen, Germany

Albert P. H. Goede
Space Research Organization of the Netherlands, Utrecht, The Netherlands, now at: Royal Netherlands Meteorological Institute, De Bilt, The Netherlands

Edward V. Browell and William B. Grant
NASA Langley Research Center, Hampton, VA, USA

Geoffrey C. Toon
Jet Propulsion Laboratory, Pasadena, CA, USA

Thomas Blumenstock
Institute of Meteorology and Climate Research, Forschungszentrum Karlsruhe and University of Karlsruhe, Karlsruhe, Germany

Bo Galle
Swedish Environmental Research Institute, Gothenburg, Sweden

Björn-Martin Sinnhuber and Stewart Davies
School of the Environment, University of Leeds, Leeds, UK

Abstract

Denitrification has been studied using measurements of stratospheric HNO_3 and N_2O by the Airborne SUbmillimeter Radiometer ASUR, operated on board the NASA DC-8 during THESEO 2000 / SOLVE. Lidar measurements taken on board the same aircraft have been used to distinguish between temporary uptake of HNO_3 in polar stratospheric clouds (PSCs) and denitrification events. To derive an NO_y budget, $ClNO_3$ data by balloon borne and ground-based Fourier transform infrared measurements and a model estimate of NO_x+$2N_2O_5$ have been considered. The HNO_3 profiles of sporadic ASUR measurements without PSC coverage in January suggest that denitrification had started in the vortex core region by then. Vortexwide

denitrification was found in mid-March 2000. Corrected for diabatic descent using the N_2O measurements, a vortex averaged NO_y deficit between 1.2 $\pm$0.9 ppb at about 16 km altitude and 5.3 $\pm$2.7 ppb at about 20.5 km altitude was derived compared to December 1999, based on an observed decrease in HNO_3 between 2.2 and 3.5 ppb during this time period. A shift in the NO_y partitioning from HNO_3 towards $ClNO_3$ of about 0.4 to 0.7 ppb was observed in mid-March compared to December, indicating that chlorine deactivation was occurring. Comparisons with the SLIMCAT 3D chemical transport model applying denitrification schemes based on ice and nitric acid trihydrate particles in equilibrium, respectively, reveal agreement within the error bars at higher altitudes ($\sim$ 19 km) but show discrepancies at lower altitudes ($\sim$ 16 km). It is suggested that more sophisticated denitrification schemes are needed to generally describe denitrification processes.

1. Introduction

Denitrification is the irreversible removal of reactive nitrogen from the polar stratosphere by the sedimentation of particles containing HNO_3.

HNO_3 in the stratosphere is mainly formed by the reaction

$$NO_2 + OH + M \rightarrow HNO_3 + M, \quad (1)$$

where M is a molecule that is not changed by the reaction. Further sources of HNO_3 can be heterogeneous reactions on liquid aerosol and / or polar stratospheric clouds (PSCs), like

$$ClNO_3 + HCl_{(s)} \rightarrow Cl_2 + HNO_{3(s)}, \quad (2)$$

$$N_2O_5 + HCl_{(s)} \rightarrow ClNO_2 + HNO_{3(s)}, \quad (3)$$

$$N_2O_5 + H_2O_{(s)} \rightarrow 2HNO_{3(s)}, \quad (4)$$

$$ClNO_3 + H_2O_{(s)} \rightarrow HOCl + HNO_{3(s)}. \quad (5)$$

It is destroyed by photolysis

$$HNO_3 + h\nu \rightarrow OH + NO_2 \quad (6)$$

and by the reaction with OH

$$HNO_3 + OH \rightarrow NO_3 + H_2O. \quad (7)$$

The time scale for the gas-phase reactions is several days and leads to a seasonal variation in HNO_3 mixing ratio that increases with latitude [Gille et al. 1996, Santee et al., 1999]. The photolysis of HNO_3 in polar spring releases NO_2 which deactivates chlorine by the reaction

$$ClO + NO_2 + M \rightarrow ClNO_3 + M. \quad (8)$$

Removal of HNO_3 from the polar stratosphere by denitrification therefore slows down chlorine deactivation and leads to prolonged ozone destruction and enhanced ozone loss [Rex et al., 1997, Waibel et al., 1999,
Tabazadeh et al., 2000].

Because of the colder and more stable vortex conditions, perturbations in HNO_3 due to denitrification are a more common feature in the Antarctic than in the Arctic vortex [Fahey et al., 1990, Roche et al., 1994, Santee et al., 1995, 1999]. However, denitrification events in recent Arctic winters have been reported applying satellite borne, balloon borne and airborne techniques [Sugita et al., 1998, Rex et al., 1999, Kondo et al., 2000].

Denitrification in the Arctic vortex in winter 1999 / 2000 was first suggested by Santee et al. [2000] based on measurements of the Microwave Limb Sounder on board the UARS satellite. Popp et al. [2001] studied denitrification using NO_y in situ measurements from the high altitude aircraft ER-2 with an NO_y-N_2O correlation. Here a different approach is presented, which is based on remote measurements of HNO_3 and N_2O performed by the Airborne SUbmillimeter Radiometer ASUR between December 1999 and March 2000. As N_2O has a lifetime of more than one year below 33 km altitude [WMO, 1986] we use N_2O as a dynamical tracer to correct for diabatic descent inside the vortex. We discuss the development and distribution of HNO_3 and address changes in the NO_y partitioning by using balloon borne and groundbased Fourier transform infrared (FTIR) measurements of $ClNO_3$ and a model estimate of $NO+NO_2+2N_2O_5$. In the following we define NO_y as $HNO_3 + ClNO_3 + NO + NO_2 + 2N_2O_5$ as other odd nitrogen species have negligible contributions at the considered accuracy. We quantify denitrification in the Arctic vortex and study the structure of denitrification in altitude and equivalent latitude. Finally we compare the results with calculations by a chemical transport model that apply a denitrification scheme based on ice, a denitrification scheme based on nitric acid trihydrate (NAT) particles in equilibrium, or no denitrification scheme.

2. Measurements

2.1. Airborne measurements of HNO_3 and N_2O

Measurements of HNO_3 and N_2O were performed by the Airborne SUbmillimeter Radiometer ASUR [von König et al., 2000]. ASUR is a passive heterodyne radiometer developed in 1991 [Crewell et al., 1994, Wehr et al., 1995]. It operates in single sideband mode. Since 1994 it uses a liquid helium cooled SIS (superconductor-insulator-superconductor) detector [Mees et al., 1995, de Valk et al., 1997]. System noise temperatures between 550 and 1450 K are achieved, depending on the measured frequency. Since 1998 a frequency range from 604.3 to 662.3 GHz is covered by ASUR, and continuous tuning within this frequency band is possible. Apart from HNO_3 and N_2O, several other trace gases important for the ozone chemistry, such as HCl, ClO, and ozone, can be measured. Signatures of HO_2, CH_3Cl and water vapor can also be detected. For spectral analysis of the signals, an acousto-optical spectrometer (AOS) with a

band width of 1.5 GHz and a resolution of 1.5 MHz is used [Rosolen et al., 1994].

The ASUR instrument is designed to operate on board an aircraft flying near the tropopause to avoid signal absorption of tropospheric water vapor. During the THESEO 2000 / SOLVE campaign, ASUR was operated on board NASA's DC-8 research aircraft. Twenty-three research flights were performed in the Arctic polar region during three deployments (from Nov. 30 to Dec. 16, 1999, from Jan. 14 to Jan. 29, 2000, and from Feb. 27 to Mar. 15, 2000). ASUR was observing to the right hand side of the aircraft with a constant elevation angle of 12°.

The pressure broadening of the detected emission lines allows the retrieval of vertical profiles of volume mixing ratio (VMR) of the measured species. To achieve a sufficient signal-to-noise ratio, the individually measured spectra are integrated over a time span of about 100 seconds in the case of HNO_3, and about 150 seconds in the case of N_2O. The retrieval is based on the optimal estimation method (OEM) [Rodgers, 1976, 1990]. This method allows to use a priori information to stabilize the solution. Temperature and pressure data for the retrieval were taken from analyses by the Data Assimilation Office (DAO), interpolated on the DC-8 flight path. For the N_2O retrieval, a line at 652.8 GHz is used, the a priori information for the OEM is based on an average of profiles obtained by the SLIMCAT chemical transport model (see section 3.1) with a constant a priori error of 90 ppb. The HNO_3 retrieval uses a rotational band around 606.8 GHz, in this case a zero a priori with a constant a priori error of 10 ppb is sufficient to obtain stable results [von König, 2001]. In both cases the considered lines are located on wings of ozone lines, so ozone is retrieved simultaneously with HNO_3 or N_2O.

The profile retrieval is performed on equidistant altitude levels of two kilometers spacing. The retrieved vertical profiles have an altitude resolution of typically 6-10 km in the lower stratosphere, defined by the full width at half maximum (FWHM) of the averaging kernel functions. The averaging kernels of typical HNO_3 and N_2O measurements of the instrument are shown in figure 1. The averaging kernel function of a certain altitude level shows the contribution of other altitudes to the retrieved value at this altitude level. The sum of the averaging kernels for a given altitude (dashed line in fig. 1) shows the information content of the measurement. Values around one indicate that there is sufficient information in the measurement, values lower than 0.5 indicate that the retrieval is dominated by a priori information. It can be seen that a retrieval is possible between about 15 and 40 km altitude in the case of N_2O, and between about 15 and 35 km altitude in the case of HNO_3. The horizontal resolution of ASUR measurements is determined by aircraft speed and the integration time required to achieve a sufficient signal-to-noise ratio. For HNO_3 values around 20 km, for N_2O values around 30 km are typically achieved. The precision of the measurements is determined by the signal-to-noise ratio and is estimated to be around 0.3 ppb for HNO_3 and 15 ppb for N_2O. The accuracy is mainly determined by the spectroscopic parameters of the lines, the accuracy of the used temperature and pressure data, and the signal-to-noise ratio. The accuracy of N_2O is estimated to be 30 ppb or 15%, which ever is higher. This is supported by comparisons with in situ measurements by high altitude aircraft [Greenblatt et al., 2002]. It is noted that the a priori influence on the retrieval of N_2O is still in the order of 10% around 15 - 17 km altitude (fig. 1). However, comparisons of ASUR N_2O profiles with in situ measurements show agreement well within the accuracy also at these altitudes in the Arctic vortex 1999/2000 [Greenblatt et al. 2002]. The accuracy of the HNO_3 measurements is estimated to be 0.6 ppb or 15%, which ever is higher. Comparisons with balloon borne and ground-based FTIR measurements [von König, 2001] show that this is a conservative estimate.

2.2. Airborne measurements of polar stratospheric clouds (PSCs)

To distinguish between temporary uptake of HNO_3 from the gas phase into PSCs and denitrification events, aerosol measurements by the Langley airborne Differential Absorption Lidar (DIAL) [Browell et al., 1998] are used. DIAL uses wavelengths at 1064 nm and 603 nm to determine the aerosol scattering ratio. DIAL aerosol measurements cover an altitude range up to 30 km with a vertical resolution of 225 m. A horizontal resolution of 42 km is achieved and the measurement accuracy is estimated to be better than 3%.

DIAL was operated on board the DC-8 throughout the THESEO 2000 / SOLVE campaign, observing in zenith looking geometry.

2.3. Balloon borne and ground-based measurements of $ClNO_3$

As a significant part of the NO_y in the stratosphere can be present as $ClNO_3$ in spring vortex conditions

after chlorine deactivation, data from the MkIV interferometer as well as ground-based Fourier Transform Infra-Red (FTIR) instruments at Kiruna and Harestua are used to constrain this contribution.

The MkIV interferometer [Toon, 1991] is a high resolution FTIR spectrometer. It can be operated from a balloon, taking absorption spectra in solar occultation geometry against the Earth's limb during sunrise or sunset, and also from the ground with uplooking geometry. The MkIV instrument uses a Michelson interferometer covering a frequency range between 650 and 5650 cm^{-1}, at a spectral resolution of 0.01 cm^{-1}. A balloon borne sunrise or sunset measurement in limb occultation mode results in vertical profiles of more than 30 different trace gases with a vertical resolution of about 2 km. Assuming no significant horizontal gradients in atmospheric composition, the accuracy of these profile measurements are determined by uncertainties in the spectroscopic parameters which are estimated to be about 5% for $ClNO_3$. Spectroscopic data for all $ClNO_3$ measurements presented have been taken from Birk and Wagner [2000] which give a better consistency for different bands and a more realistic chlorine budget in the stratosphere [Oelhaf et al., 2001].

During the THESEO 2000 / SOLVE campaign, MkIV performed two balloon flights on board the OMS remote gondola from Esrange (67.9°N, 21.1°E). The first balloon launch occurred on December 3, 1999, where a sunset occultation was observed. The second launch was on March 15, 2000 when a sunrise occultation was observed. The balloon measurements covered an altitude range between 6 and 34 km in December, while in March profiles between 12 and 30 km altitude were obtained. Both flights had tangent points well inside the polar vortex in the lower stratosphere.

In addition to the two balloon measurements, MkIV performed 22 days of ground-based column measurements of $ClNO_3$ during the winter 1999 / 2000 from Esrange. Further ground-based FTIR instruments were operated at Kiruna (67.8°N, 20.4°E) and Harestua
(60.2°N, 10.8°E) during this winter. The spectrometer at Kiruna is a Bruker 120 HR with a spectral range from 700-4500 cm^{-1} and a spectral resolution of 0.0025 cm^{-1}. The instrument at Harestua is a Bruker 120 M Fourier Transform Spectrometer. It covers a frequency range of 600-4500 cm^{-1} at a resolution of 0.0035 cm^{-1}. For further information on measurement technique and data analysis with these instruments the reader is referred to Blumenstock et al. [1997] and Galle et al. [1999], respectively. Apart from errors in the spectroscopic parameters the accuracies of the column measurements depend mainly on uncertainties in the assumed VMR profile shapes, the temperature profiles, and the observation angle. These latter factors are estimated to result in an error of no more than 7%.

To obtain vortexwide $ClNO_3$ information that is comparable to the ASUR HNO_3 profiles we use the ground-based measurements. The $ClNO_3$ column measurements do not show large variations within the considered time periods in December 1999 and March 2000 and the columns derived by integrating the MkIV balloon profiles, extended by SLIMCAT $ClNO_3$ at altitudes were no measurement information was available, agree well with the ground-based columns. So the MkIV profiles from December and March, respectively, are scaled below 26 km until the resulting profiles have the same column abundances as the ground-based measurements. The altitude of 26 km was chosen as most PSCs were found below this altitude and changes in $ClNO_3$ are expected to be mainly caused by chlorine activation due to heterogeneous reactions and chlorine deactivation. Above this altitude the partial column abundance is kept constant. The uncertainties introduced by this method are mainly caused by the uncertainty in the partial column above 26 km, as well as by the uncertainty of the partial column below 12 km in March. These uncertainties can be quantified to introduce an error of 2.5 % and 3.5 %, respectively. This leads to an accuracy of about 18 % for the quantities presented in this study that are derived by this method. The resulting profiles are folded to ASUR's altitude resolution using the averaging kernel functions of the HNO_3 measurements by ASUR.

3. Models

3.1. The SLIMCAT model

SLIMCAT is a three-dimensional chemical transport model (CTM) [Chipperfield, 1999]. It calculates homogeneous chemistry and photochemistry as well as heterogeneous chemistry on liquid aerosols, NAT, and ice. The composition of liquid aerosols is calculated according to Carslaw et al. [1995a, 1995b], NAT is formed at the equilibrium NAT-existence temperature according to Hanson and Mauersberger [1988]. The model is forced by temperatures and horizontal wind fields from analyses by The Met. Office, UK

(UKMO), while vertical advection is calculated from heating rates [Shine, 1987]. The model runs with a horizontal resolution of 7.5 ° longitude × 5 ° latitude on 18 isentropic levels, leading to a vertical resolution of about 1 km in the lower stratosphere. The data for early-December were obtained by a model run that was initialized for October 1991 by a 2-D model. Three new model runs were started for December 8, 1999, initialized by the previous run but using different denitrification schemes.

The first model run includes a simple denitrification scheme [Chipperfield, 1999] in which ice is assumed to form below the ice frost point and to remove gas-phase HNO_3 as co-condensed NAT. The ice particles are assumed to have a radius of 10 μm and a fall velocity of about 1500 m/day. Above the frost point but below the NAT-existence temperature NAT particles are formed with an assumed radius of 1 μm. Denitrification in this scheme occurs effectively only due to the sedimenting ice particles containing the co-condensed HNO_3. In the second run no ice is formed but NAT is assumed to form instantaneously in two modes with radii of 0.5 μm and 6.5 μm, respectively, based on observations by Fahey et al. [2001]. For these two modes fall velocities of 1 m/day and 1100 m/day, respectively, are assumed. The maximum number density of the small mode was set to 1 cm^{-3}, condensed HNO_3 in excess was assigned to the large mode. The third run is based on the first run described in this section but with the particle sedimentation switched off. Data for March were taken from these three model runs. For a more detailed description of these schemes the reader is referred to Davies et al. [2002].

All the data shown were obtained by interpolating the SLIMCAT output to the positions of the considered measurements. For N_2O SLIMCAT vortex averages were used directly. The resulting profiles were folded to ASUR's altitude resolution and averaged in the same way the measured profiles were averaged.

3.2. Estimate of $NO_x + 2\ N_2O_5$

To close the NO_y budget, information is needed about the species $NO + NO_2$, in the following defined as NO_x, and their nighttime reservoir N_2O_5. Other NO_y constituents can be considered as negligible for a study with the aimed accuracy. For simplification we define $NO_x + 2N_2O_5$ as NO'_x. As there are no vortexwide measurements of these species, a model estimate is used, based on a steady state approach.

In the gas phase the ratio NO'_x/HNO_3 is controlled by the reactions (1), (6), and (7). This means that the ratio is mainly dependent on the history of sunlight exposure of the airmass. This can be modeled well by the SLIMCAT model. As a first order correction the heterogeneous reactions, mainly reaction (4), contribute to the NO'_x/HNO_3 ratio. As SLIMCAT tends to overestimate NO_y, we use the model to derive the NO'_x/HNO_3 ratio for each HNO_3 measurement position and calculate NO'_x from the ASUR measurement. Sensitivity studies with smoothed and non-smoothed HNO_3 profiles of SLIMCAT and MkIV show that the error introduced by ASUR's altitude resolution increases with altitude and stays below 0.5 ppb up to 25 km. Above the altitude where the ASUR HNO_3 exceeds the non-smoothed SLIMCAT HNO_3 due to altitude resolution, SLIMCAT NO'_x is used. This was usually around 33 km in December and around 27 km in March. The influence of the SLIMCAT NO'_x to the altitude range considered in the following is small (< 0.4 ppb) in March. In December there is a significant influence at the upper end of the altitude range (~ 1.7 ppb at 25 km) due to high NO'_x VMRs (up to 14 ppb) between 30 and 40 km. This influence is decreasing with decreasing altitude. However, some averaging kernels from 30-40 km result in slightly negative values in the smoothed NO'_x profiles at low altitudes (< 21 km).

In March a good agreement between the derived NO'_x, calculated using the MkIV HNO_3 and the SLIMCAT NO'_x/HNO_3, and the NO'_x observed by MkIV is achieved. The derived NO'_x VMR stays within 1 ppb of the observed NO'_x VMR up to an altitude of 28 km. After folding to ASUR's altitude resolution, an error below 0.2 ppb up to 17 km and below 0.5 ppb up to 20 km can be estimated. However, in December the agreement with MkIV is less good. The observed NO'_x VMR stays close to zero up to 24 km altitude, then rises to about 8.5 ppb at 30 km while the derived NO'_x stays close to zero up to 26.5 before it starts to rise, resulting in an offset of about 2.5 km up to 30 km altitude. Recent studies of NO_y partitioning show discrepancies between measurements and models concerning the NO_2/HNO_3 ratio [Sen et al., 1998] and the NO_x/NO_y ratio [Jucks et al., 1999] at higher altitudes, especially under conditions of low aerosol loading. It is likely that this happens as well when the SLIMCAT model is used. A possible reason for the discrepancy in December might be a problem with the accurate calculation of the heterogeneous reactions, which might have an increased relative importance due to the lack of sun-

light. Sensitivity studies using the MkIV measurement as well as the references above indicate, that an error of less than 0.5 ppb up to 19 km, 1 ppb up to 21 km, and 2 ppb up to 25 km is a conservative estimate for the uncertainty of the calculated NO_x' in December, after folding to ASUR's altitude resolution.

4. Results

4.1. Development of N_2O, HNO_3, and potential PSC-area

The vortex in the Arctic winter 1999 / 2000 was very stable and characterized by cold temperatures [Manney and Sabutis, 2000]. In the following discussion we use a vortex edge definition by Nash et al. [1996]. We determine the vortex boundary region by the local maximum convex and concave curvature in the distribution of Ertel's potential vorticity (PV) on equivalent latitudes at a potential temperature of 475 K. Equivalent latitude is a measure of the area enclosed by a PV isoline, where this area is assumed to be circular and centered around the pole. The potential vorticity data were taken from analyses by the European Center for Medium Range Weather Forecast (ECMWF). We use the inner edge of this boundary region as the vortex edge. The vortex area defined by this method for the times of the three deployments and in between are given in figure 2 a). Calculating the edge numerically gives stable results from day -20 of year 2000 onwards, where the vortex edge is located at 65° equivalent latitude. For the days before day -20 the vortex edge has been set to this value as well. This is supported by the horizontal distribution of N_2O observed by ASUR in December 1999 [Bremer et al., 2002]. Instabilities in the numerical calculation were found around day -15 and -5, respectively, as well as around day 50, resulting from an inhomogeneous PV-equivalent latitude distribution. However, studies of the variations in HNO_3 and N_2O measurements up to day -15 and reverse domain filling trajectory calculations for the subsequent days (not shown) do not suggest that this has a significant influence on the quantities derived in this study. For the rest of the time the vortex edge could be well determined by this method. It can be seen in figure 2 a) that the vortex loses about 40% of its area during the winter.

Figure 2 b) shows mean altitudes of the 100 ppb and the 200 ppb level of N_2O inside the vortex. To create these means the values were weighted with the area of the equivalent latitude band in which they were measured. This method has been applied to all averages presented, as the observed variations were dependent on equivalent latitude in the first approximation. The crosses indicate mean altitudes on each flight, with the vertical bars giving the standard deviation, reflecting the variation observed during the flight. The horizontal bars indicate the averages over one deployment while the dashed lines show linear interpolations between the deployments. We use N_2O as a dynamical tracer to detect diabatic descent in the polar vortex. The descent of the 100 ppb and 200 ppb N_2O levels is clearly visible in figure 2 b). The 200 ppb level descends from an altitude of 18.3 km in the first half of December 1999 to an altitude of 16 km in the first half of March 2000. The 100 ppb level descends from 22 km to about 19 km. It is noted that the scattering of the diurnal means is very small in March 2000 but larger in December 1999 and especially in January 2000. A more comprehensive description of diabatic descent using ASUR N_2O can be found in Bremer et al. [2002].

The evolution of HNO_3 over the winter is shown in figures 2 c) for the 100 ppb N_2O level and 2 d) for the 200 ppb N_2O level. Changes due to diabatic descent are corrected by plotting the HNO_3 values over the N_2O campaign means. Crosses indicate flight means inside the vortex, the vertical bars give the standard deviation. In December, values around 9.5 ppb HNO_3 at the 100 ppb level of N_2O and 8 ppb HNO_3 at the 200 ppb level of N_2O are observed. In January the variation in the diurnal means was very high. As extensive PSC coverage was observed by DIAL in January, the variations are likely to be caused by uptake of gas-phase HNO_3 into PSCs. This process has been observed and described in literature [e. g. Dessler et al., 1999, von König et al., 2002]. In March the HNO_3 values had decreased considerably, with mean volume mixing ratios (VMRs) of slightly more than 6 ppb on both considered N_2O levels.

To distinguish between temporary uptake of HNO_3 into PSCs and irreversible removal of HNO_3 by the sedimentation of HNO_3-containing particles, DIAL data are used. The occurrence of a PSC is diagnosed when the aerosol scattering ratio exceeds a threshold of 0.6 in the infrared channel and a threshold of 0.17 in the visible channel. The different observation angles of DIAL and ASUR were taken into account by applying a time window of 300 seconds before and after a PSC detection by DIAL, corresponding to 70 km at typical aircraft speed. This is roughly the distance between the observation points of DIAL and ASUR at the altitude up to which PSCs were observed. As

the PSCs observed during SOLVE had usually large horizontal dimensions compared to this distance, the probability to observe a significant portion of "PSC-contaminated" air without recognizing it with the lidar is comparatively small. Applying this rigid criterion to the ASUR HNO_3 measurements inside the vortex in January, measurements on five different flight days remain. These measurements are rather sparse and cannot be considered as vortex averages. The averages of these measurements are shown as diamonds in figures 2 c) and d). The measurements taken on the days 14, 23 and 29 show higher VMRs of HNO_3 than the average December values. This is expected as a high chlorine activation was observed in the January vortex (see e.g. [Bremer et al., 2002]). According to figure 4, a $ClNO_3$ VMR around 1 ppb was observed in the lower stratosphere in early-December. This would lead to an increase of 1 ppb of gas-phase HNO_3 by reaction (2) after the evaporation of PSC-particles if $ClNO_3$ was fully converted. A further increase could be caused by the conversion of N_2O_5 into HNO_3 by reactions (3) and (4).

However, the measurements on the days 16 and 20 show a lower HNO_3 VMR. Especially on day 20 the value at 100 ppb N_2O falls below the value at 200 ppb N_2O. This suggests that these airmasses have been partially denitrified. It has to be noted that the measurements on the days 14, 23 and 29 were taken at equivalent latitudes between 67.5° and 73°, very close to the vortex boundary region during these days, while the measurements on the days 16 and 20 were located near 85° equivalent latitude. As one would rather expect lower HNO_3 near the vortex edge than in its core region due to photolysis, it is likely that denitrification had started to occur in the vortex core region by mid-January.

Figure 2 e) shows the potential PSC area on the 100 and 200 ppb N_2O levels. The potential PSC area was defined as the area below the temperature of the existence of nitric acid trihydrate (NAT). The NAT-existence temperature was calculated using the formula by Hanson and Mauersberger [1988]. The calculation is based on a VMR of 5 ppm H_2O, which was reasonable for the lower stratosphere in that winter [Schiller et al., 2002], and on the HNO_3 VMR measured by ASUR. For the times between the campaigns, interpolations between the campaign means (dashed lines in figure 2 b), c), and d)) were used. The area was calculated using temperatures from the ECMWF. It can be seen that PSCs were expected to occur during all three campaign deployments, with a maximum area of $13.5 \cdot 10^6$ km^2 in mid-January on both considered N_2O levels. The use of the HNO_3 measurements without PSC coverage in January (diamonds in figure 2 c) and d)) would increase the potential PSC area by less than $1 \cdot 10^6$ km^2. Potential PSC occurrence ceased around day 73.

The area below the frost point is shown in figure 2 f), based on an H_2O VMR of 5 ppm and ECMWF temperatures. Ice PSCs were mainly expected during two major events at the end of December and mid-January, where the area below the frost point reached $2.3 \cdot 10^6$ km^2 on the 100 ppb N_2O level. The maximum area on the 200 ppb level was $0.6 \cdot 10^6$ km^2. It has to be noted that temperatures from UKMO analyses near the frost point were about 2 K lower than ECMWF analyses. This lead to a significantly larger potential ice area derived from UKMO analyses (about $5 \cdot 10^6$ km^2 on the 460 K isentrope during these two major events) while the potential PSC area was similar in the two analyses [Davies et al., 2002].

4.2. Distribution of HNO_3 and $ClNO_3$ inside the vortex

Figure 3 shows the distribution of HNO_3 and $ClNO_3$ versus equivalent latitude in December 2-5, 1999 as well as in March, 9-15, 2000. These time spans were chosen to obtain a reasonable coverage of the vortex with HNO_3 and $ClNO_3$ measurements. The HNO_3 measurements were selected to be at positions without PSC occurrence using the criterion described above. At the beginning of December HNO_3 shows an increase with equivalent latitude from 8 ppb in the vortex boundary region, located at equivalent latitudes below 65°, to more than 11 ppb in the vortex core, at altitudes around 22 km. This behavior is expected as photolysis of HNO_3 is reduced due to the lack of sunlight in the beginning of the polar night. The distribution in March shows the opposite tendency. The highest values, above 8 ppb are now found in the vortex boundary region, located at equivalent latitudes smaller than 70° in mid-March. Poleward of 73° the HNO_3 VMR is drastically reduced and maximum values below 6 ppb are dominant beyond 80° at about 17 km altitude.

In the lower panels of figure 3, $ClNO_3$ columns measured by different ground-based FTIR instruments are shown. Additionally the $ClNO_3$ profiles from the two balloon flights of the MkIV instrument were integrated and extended by SLIMCAT profiles to derive columns. An average column abundance of $(1.61 \pm 0.11) \cdot 10^{15}$ molec./cm^2 was found inside the

vortex in December. The abundance in March was significantly higher with values of $(3.53 \pm 0.16) \cdot 10^{15}$ molec./cm^2. The errors give the standard deviation about the averages, the statistical uncertainty of the mean $ClNO_3$ values. The enhanced $ClNO_3$ values in March indicate that chlorine deactivation has taken place, qualitatively consistent with ASUR observations of HCl and ClO described in Bremer et al. [2002]. The variation with equivalent latitude within the two considered periods is small. The formation of a $ClNO_3$ collar [Chipperfield et al., 1997], which is a common feature during chlorine deactivation, has apparently been overcome by the time of observation.

4.3. Odd Nitrogen budget and denitrification

To understand the differences in the observed HNO_3 and their relation to denitrification, we derive NO_y by the means stated in sections 2 and 3.2. The results are shown in the top row of figure 4. They show vortex averages of the different NO_y constituents as well as of NO_y itself. The profiles are plotted versus N_2O measurements by ASUR. Black profiles represent data from December 2-5, 1999, gray profiles represent data from March 9-15, 2000. To derive the altitude of a certain VMR, the corresponding N_2O profile has to be considered (left column in figure 4). Between the considered time periods we observe a diabatic descent from 18.5 to 16 km on the 200 ppb level of N_2O and from 22 to about 19 km on the 100 ppb level. Corrected for this diabatic descent we observe a decrease of 3.5 ppb HNO_3 between 100 and 50 ppb N_2O in the vortex average. Below 100 ppb the decrease is slightly lower, reaching 2.2 ppb at 200 ppb N_2O. The increase in $ClNO_3$, observed by the FTIR instruments, corresponds to an increase between 0.4 and 0.7 ppb in the considered altitude range, as seen with ASUR's altitude resolution. Using the estimate of $NO_x+2N_2O_5$ we obtain a significant deficit in the NO_y mixing ratio reaching from 1.2±0.9 ppb at 200 ppb N_2O to 5.3±2.7 ppb at 50 ppb N_2O that is interpreted as denitrification. The errors give the estimated accuracies obtained by propagating the statistical errors and the estimated systematic errors through the calculation.

To further examine the structure in the HNO_3 distribution inside the vortex, we derive ΔNO_y for measurements between 85° and 80° equivalent latitude, between 80° and 75° equivalent latitude, and between 75° equivalent latitude and the vortex edge (which was located around 70° equivalent latitude in mid-March). We use the average over the December vortex and derive ΔNO_y as the difference between these regions in March and the December average, corrected for diabatic descent. Figure 5 shows ΔNO_y for these regions on the 16 km altitude level, which corresponds to roughly 200 ppb ASUR N_2O in March, and on the 19 km altitude level, corresponding to 100 ppb ASUR N_2O. In the March HNO_3 measurements we find a trend of decreasing HNO_3 with increasing equivalent latitude (see section 4.2). This trend is found in the NO_y as well, which means that the NO_y deficit increases with equivalent latitude at the considered altitude levels.

4.4. Comparisons with the SLIMCAT model

Comparisons of these observations with the different runs of the SLIMCAT model are shown in the rows 2-4 of figure 4. Both runs with denitrification schemes calculated a considerable denitrification which is in agreement with the observed NO_y deficit within its accuracies at the upper end of the considered altitude range. However, the SLIMCAT ice run calculated less NO_y deficit than observed, which is evident at the lower end of the considered altitude range, while the SLIMCAT NAT run calculated a significantly larger NO_y deficit than observed at lower altitudes. The trend of increasing NO_y deficit with equivalent latitude inside the vortex shown in figure 5 is basically reproduced by the SLIMCAT ice run. The NAT run shows a more uniform distribution of denitrification over the vortex, especially at 16 km.

It should be noted that SLIMCAT underestimated diabatic descent in winter 1999 / 2000 when compared to the descent derived from ASUR N_2O measurements. Applying the measured diabatic descent by ASUR to the SLIMCAT NO_y would increase the NO_y deficit by about 0.7 ppb in both runs with denitrification.

Looking at the non-denitrified run of the SLIMCAT model in figure 4 one can see that, though considerably smaller, a loss in HNO_3 is present there as well. Unlike in the denitrified run, this loss is basically completely compensated by the increase in $ClNO_3$. The NO_y deficit is not exactly zero which is mainly caused by the effect of smoothed profiles.

Denitrification derived from NO_y in situ observations from the high altitude aircraft ER-2 over the winter [Popp et al., 2001] has been compared with the same model runs and shows best agreement with the SLIMCAT NAT run, when all ER-2 flights (January 14 - March 12, 2000) are taken into account. However, when only the flights in mid-March are considered, the SLIMCAT NAT run shows the tendency to

calculate too much denitrification at lower altitudes compared to the ER-2 measurements as well [Davies et al., 2002]. The winter 1999 / 2000 was the first winter in which extensive denitrification was calculated by SLIMCAT in the Arctic using a denitrification scheme based on ice [Sinnhuber et al., 2000]. However, the denitrification calculated with the ice scheme was very sensitive to the temperature differences between UKMO and ECMWF meteorological analyses in this winter (see section 4.1). Forcing the model with ECMWF analyses yielded less than half of the NO_y deficit calculated with UKMO (not shown). The discrepancies between the NAT run and the observations this winter and between the ice run and observations this winter (see also [Davies et al., 2002]) together with the indications for an underestimation of denitrification in earlier winters [Sinnhuber et al., 2001] suggest that the presented model approaches might be to simple to give a general description of denitrification.

5. Summary and conclusions

We studied denitrification inside the Arctic vortex in winter 1999 / 2000 based on measurements of HNO_3 and N_2O by the Airborne SUbmillimeter Radiometer ASUR, flying on board the NASA DC-8 during THESEO 2000 / SOLVE. Measurements of the aerosol scattering ratio by the DIAL lidar on board the same aircraft were used to identify PSCs and to distinguish between temporary uptake of gas-phase HNO_3 into PSCs and denitrification events. Measurements of $ClNO_3$ by the MkIV balloon instrument and ground-based FTIR instruments, as well as a model estimate of $NO_x+2N_2O_5$, were used to evaluate changes in the NO_y partitioning.

The HNO_3 profiles of sporadic measurements of ASUR without PSC coverage during the January campaign suggest that denitrification processes had started in the vortex core (around 85° equivalent latitude) by then. No indication of denitrification near the vortex edge was found during January.

A vortexwide decrease in HNO_3 was found during the March campaign. The NO_y budget, derived using the ancillary measurements and estimates above, showed a vortex averaged NO_y deficit between 1.2 $\pm$0.9 ppb at about 16 km altitude and 5.3 $\pm$2.7 ppb at about 20.5 km altitude between early-December and mid-March that can be attributed to denitrification. To calculate the NO_y deficit a diabatic descent of about 3 km at the 100 ppb N_2O level and about 2.5 km at the 200 ppb N_2O level during this time period was taken into account, derived from ASUR N_2O measurements. The NO_y deficit was mainly based on loss of HNO_3. A vortex averaged decrease of about 3.5 ppb between 19 km and 20.5 km, going down to about 2.2 ppb at 16 km altitude, was observed by the ASUR instrument. However, a significant portion (about 0.4 to 0.7 ppb) of HNO_3 had been converted to $ClNO_3$ due to chlorine deactivation in March, thus reducing the effect of the HNO_3 decrease when the NO_y budget is considered.

A trend of stronger denitrification with increasing equivalent latitude was found inside the vortex in mid-March.

The observations were compared with runs of the SLIMCAT model applying different denitrification schemes based on ice and on large NAT particles in equilibrium, respectively. Both model runs produced widespread, significant denitrification. While agreement within the accuracies of the NO_y deficit derived from the observations is achieved at higher altitudes ($\sim$ 19 km), the ice run underestimates and the NAT run significantly overestimates the NO_y deficit at lower altitudes ($\sim$ 16 km) in mid-March.

It is expected that future models based on more sophisticated denitrification schemes that include denitrification based on large HNO_3-containing particles in a non-equilibrium state [Fahey et al., 2001, Carslaw et al., 2002] will improve our capability of modeling the denitrification in the Arctic polar stratosphere.

Acknowledgments. We would like to acknowledge G. Näveke for his excellent technical support before and during the flight campaigns, I. Wohltmann for providing the vortex edge calculations, J. Mellqvist for a reanalysis of the $ClNO_3$ data from Harestua, M. P. Chipperfield for support with the SLIMCAT model, as well as DAO, ECMWF, and UKMO for providing meteorological analyses. We would further like to thank the European Union for funding our campaign activities (Contract no. EVK2-CT-1999-00047), NASA for the opportunity to participate on board the DC-8, and the aircraft crew for their excellent support.

References

Birk, M., and G. Wagner, A new spectroscopic database for chlorine nitrate, paper presented at 6th HITRAN Conference, Cambridge, USA, June 2000.

Blumenstock, Th., H. Fischer, A. Friedle, F. Hase, and P. Thomas, Column amounts of $ClONO_2$, HCl,

HNO_3, and HF from ground-based FTIR measurements made near Kiruna, Sweden, in late winter 1994, *J. Atm. Chem., 26,* 311, 1997.

Bremer, H., M. von König, A. Kleinböhl, H. Küllmann, K. F. Künzi, K. Bramstedt, J. P. Burrows, K.-U. Eichmann, M. Weber, and A. P. H. Goede, Ozone depletion observed by ASUR during the Arctic Winter 1999/2000, *J. Geophys. Res.,* in press, 2002.

Browell, E. V., S. Ismail, and W. B. Grant, Differential Absorption Lidar (DIAL) measurements from air and space, *Appl. Phys. B, 67,* 399-410, 1998.

Carslaw, K. S., B. P. Luo, and T. Peter, An analytic expression for the composition of aqueous HNO_3-H_2SO_4 stratospheric aerosols including gas-phase removal of HNO_3, *Geophys. Res. Lett., 22,* 1877-1880, 1995a.

Carslaw, K. S., S. L. Clegg, and P. Brimblecome, A thermodynamic model of the system HCl-HNO_3-H_2SO_4-H_2O including solubilities of HBr from ¡200 K to 328 K, *J. Phys. Chem., 99,* 11557-11574, 1995b.

Carslaw, K. S., J. Kettleborough, M. J. Northway, S. Davies, R. S. Gao, D. W. Fahey, D. Baumgardner, M. P. Chipperfield, and A. Kleinböhl, A vortex-scale simulation of the growth and sedimentation of large nitric acid particles observed during SOLVE/THESEO-2000, *J. Geophys. Res.,* in press, 2002.

Chipperfield, M. P., E. R. Lutman, J. A. Kettleborough, J. A. Pyle, and A. E. Roche, Model studies of chlorine deactivation and formation of $ClONO_2$ collar in the Arctic polar vortex, *J. Geophys. Res., 102,* 1467-1478, 1997.

Chipperfield, M. P., Multiannual simulations with a threedimensional chemical transport model, *J. Geophys. Res., 104,* 1781-1805, 1999.

Crewell, S., P. Hartogh, K. F. Künzi, H. Nett, and T. Wehr, Aircraft measurements of ClO and HCl during EASOE 1991/92, *Geophys. Res. Lett., 21,* 1267-1279, 1994.

Davies, S., et al., Modeling the effect of denitrification on Arctic ozone depletion during winter 1999/2000, *J. Geophys. Res.,* in press, 2002.

Dessler, A. E., J. Wu, M. L. Santee, and M. R. Schoeberl, Satellite observations of temporary and irreversible denitrification, *J. Geophys. Res., 104,* 13993-14002, 1999.

de Valk, J. P. J. M. M., et al., Airborne heterodyne measurements of stratospheric ClO, HCl, O_3, and N_2O during SESAME 1 over northern Europe, *J. Geophys. Res., 102,* 1391-1398, 1997.

Fahey, D. W., K. K. Kelly, S. R. Kawa, A. F. Tuck, M. Loewenstein, K. R. Chan, and L. E. Heidt, Observations of denitrification and dehydration in the winter polar stratospheres, *Nature, 344,* 321-324, 1990.

Fahey, D. W., et al., The detection of large HNO_3-containing particles in the winter Arctic stratosphere, *Science, 291,* 1026-1031, 2001.

Galle, B., J. Mellqvist, D. W. Arlander, I. Fløisand, M. P. Chipperfield, and A. M. Lee, Ground-based FTIR measurements of stratospheric species from Harestua, Norway during SESAME and comparison with models, *J. Atm. Chem., 32,* 147-164, 1999.

Gille, J. C., P. L. Bailey, and C. A. Craig, Revised reference model for nitric acid, *Adv. Space Res., 18*(9/10), 125-138, 1996.

Greenblatt, J. B., et al., Experimental determination of vortex subsidence for the 1999-2000 Arctic winter, and comparison with models, *this issue,* 2002.

Hanson, D., and K. Mauersberger, Laboratory studies of the nitric acid trihydrate: Implications for the South polar stratosphere, *Geophys. Res. Lett., 15,* 855-858, 1988.

Jucks, K. W., D. G. Johnson, K. V. Chance, W. A. Traub, and R. J. Salawitch, Nitric acid in the middle stratosphere as a function of altitude and aerosol loading, *J. Geophys. Res., 104,* 26715-26723, 1999.

Kondo, Y., H. Irie, M. Koike, and G. E. Bodeker, Denitrification and nitrification in the Arctic stratosphere during the winter of 1996-1997, *Geophys. Res. Lett., 27,* 337-340, 2000.

Manney, G. L., and J. L. Sabutis, Development of the polar vortex in the 1999/2000 Arctic winter stratosphere, *Geophys. Res. Lett., 27,* 2589-2592, 2000.

Mees, J., S. Crewell, H. Nett, G. de Lange, H. van de Stadt, J. J. Kuipers, and R. A. Panhuyzen, ASUR - An Airborne SIS Receiver for Atmospheric Measurements of Trace Gases at 625 to 760 GHz, *IEEE Trans. Microwave Theory Tech., 43,* 2543-2548, 1995.

Nash, E. R., P. A. Newman, J. E. Rosenfield, and M. R. Schoeberl, An objective determination of the polar vortex using Ertel's potential vorticity, *J. Geophys. Res., 101,* 9471-9478, 1996.

Oelhaf, H., et al., Interconsistency checks of $ClONO_2$ retrievals from MIPAS-B spectra by using different bands and spectroscopic parameter sources, in

IRS 2000: Current Problems in Atmospheric Radiation, edited by W. L. Smith and Yu. M. Timofeyev, pp. 615-618, A. Deepak Publishing, Hampton, Virginia, 2001.

Popp, P. J., et al., Severe and extensive denitrification in the 1999-2000 Arctic winter stratosphere, *Geophys. Res. Lett., 28,* 2875-2878, 2001.

Rex, M., et al., Prolonged stratospheric ozone loss in the 1995/1996 Arctic winter, *Nature, 389,* 835-838, 1997.

Rex, M., et al., Subsidence, mixing, and denitrification of Arctic polar vortex air measured during POLARIS, *J. Geophys. Res., 104,* 26611-26623, 1999.

Roche, A. E., J. B. Kumer, J. L. Mergenthaler, R. W. Nightingale, W. G. Uplinger, G. A. Ely, J. F. Potter, D. J. Wuebbles, P. S. Connell, and D. E. Kinnison, Observations of lower-stratospheric $ClONO_2$, HNO_3, and aerosol by the UARS CLAES experiment between January 1992 and April 1993, *J. Atmos. Sci., 51,* 2877-2902, 1994.

Rodgers, C. D., Retrieval of atmospheric temperature and composition from remote measurements of thermal radiation, *Rev. Geophys., 14,* 609-624, 1976.

Rodgers, C. D., Characterization and error analysis of profiles retrieved from remote sounding measurements, *J. Geophys. Res., 95,* 5587-5595, 1990.

Rosolen, C., P. Dierich, D. Michet, A. Lecacheux, F. Palacin, R. Robiliard, F. Rigeaud, P. Vola, Wideband acousto-optical spectrometer, *Final report on ESA work-package 2411, Submillimeter Limb Sounder Bread-boarding,* 1994.

Santee, M. L., W. G. Read, J. W. Waters, L. Froidevaux, G. L. Manney, D. A. Flower, R. F. Jarnot, R. S. Harwood, and G. E. Peckham, Interhemispheric differences in polar stratospheric HNO_3, H_2O, ClO, and O_3, *Science, 267,* 849-852, 1995.

Santee, M. L., G. L. Manney, L. Froidevaux, W. G. Read, and J. W. Waters, Six years of UARS Microwave Limb Sounder HNO_3 observations: Seasonal, interhemispheric, and interannual variations in the lower stratosphere, *J. Geophys. Res., 104,* 8225-8246, 1999.

Santee, M. L., G. L. Manney, N. J. Livesey, and J. W. Waters, UARS Microwave Limb Sounder observations of denitrification and ozone loss in the 2000 Arctic late winter, *Geophys. Res. Lett., 27,* 3213-3216, 2000.

Schiller, C., et al., Dehydration in the Arctic stratosphere during the THESEO 2000 / SOLVE campaigns, *J. Geophys. Res.,* in press, 2002.

Sen, B., G. C. Toon, G. B. Osterman, J.-F. Blavier, J. J. Margitan, and R. J. Salawitch, Measurements of reactive nitrogen in the stratosphere, *J. Geophys. Res., 103,* 3571-3585, 1998.

Shine, K. P., The middle atmosphere in the absence of dynamical heat fluxes, *Q. J. Roy. Met. Soc., 113,* 603-633, 1987.

Sinnhuber, B.-M., et al., Large loss of total ozone during the Arctic winter of 1999/2000, *Geophys. Res. Lett., 27,* 3473-3476, 2000.

Sugita, T., Y. Kondo, H. Nakajima, U. Schmidt, A. Engel, H. Oelhaf, G. Wetzel, M. Koike, and P. A. Newman, Denitrification observed inside the Arctic vortex in February 1995, *J. Geophys. Res., 103,* 16221-16233, 1998.

Tabazadeh, A., M. L. Santee, M. Y. Danilin, H. C. Pumphrey, P. A. Newman, P. J. Hamill, and J. L. Mergenthaler, Quantifying denitrification and its effect on ozone recovery, *Science, 288,* 1407-1411, 2000.

Toon, G. C., The JPL MkIV interferometer, *Opt. Photonics News, 2,* 19-21, 1991.

von König, M., H. Bremer, V. Eyring, A. P. H. Goede, H. Hetzheim, Q. L. Kleipool, H. Küllmann, K. Künzi, An airborne submm radiometer for the observation of stratospheric trace gases, in *Microw. Radiomet. Remote Sens. Earth's Surf. Atmosphere*, Pampaloni, P., S. Paloscia (Eds.), 409-415, 2000.

von König, M., Chlorine activation and PSC formation in the Arctic stratosphere, Ph. D. thesis, Univ. of Bremen, Logos Verlag Berlin, Germany, 2001.

von König, M., et al., Using gas-phase HNO_3 as an indicator for PSC composition, *this issue,* 2002.

Waibel, A. E., Th. Peter, K. S. Carslaw, H. Oelhaf, G. Wetzel, P. J. Crutzen, U. Pöschl, A. Tsias, E. Reimer, and H. Fischer, Arctic ozone loss due to denitrification, *Science 283,* 2064-2069, 1999.

Wehr, T., S. Crewell, K. F. Künzi, J. Langen, H. Nett, J. Urban, and P. Hartogh, Remote sensing of ClO and HCl over northern Scandinavia in winter 1992 with an airborne submillimeter radiometer, *J. Geophys. Res., 100,* 20957-20968, 1995.

World Meteorological Organization, Scientific Assessment of Ozone Depletion: 1985, Global Ozone Research and Monitoring Project, *Report No. 16,* 1986.

Armin Kleinböhl, Bremer, H., von König, M., Küllmann, H., and Künzi, K. F., Institut für Umweltphysik, Universität Bremen, P. O. Box 330 440, 28334 Bremen,

Germany. (e-mail: kleinb@iup.physik.uni-bremen.de)

Goede, A. P. H., Space Research Organisation of the Netherlands, Sorbonnelaan 2, 3584 CA Utrecht, The Netherlands, present address: Royal Netherlands Meteorological Institute (KNMI), P.O.Box 201, 3730 AE De Bilt, The Netherlands.

Browell, E. V., and Grant, W. B., Mail Stop 401A, Langley Research Center, National Aeronautics and Space Administration, Hampton, VA 23681-2199, USA.

Toon, G. C., Mail Stop 183-601, Jet Propulsion Laboratory, California Institute of Technology, 4800 Oak Grove Drive, Pasadena, CA 91109-8099, USA.

Blumenstock, Th., Institut für Meteorologie und Klimaforschung, Forschungszentrum Karlsruhe and Universität Karlsruhe, P.O.Box 3640, 76021 Karlsruhe, Germany.

Galle, B., Swedish Environmental Research Institute, P. O. Box 47086, 40258 Gothenburg, Sweden.

Sinnhuber, B.-M., and Davies, S., School of the Environment, University of Leeds, Leeds, LS2 9JT, UK.

Received July 5, 2001; revised February 5, 2002; accepted February 5, 2002.

This preprint was prepared with AGU's LaTeX macros v5.01. File deni formatted April 24, 2002.

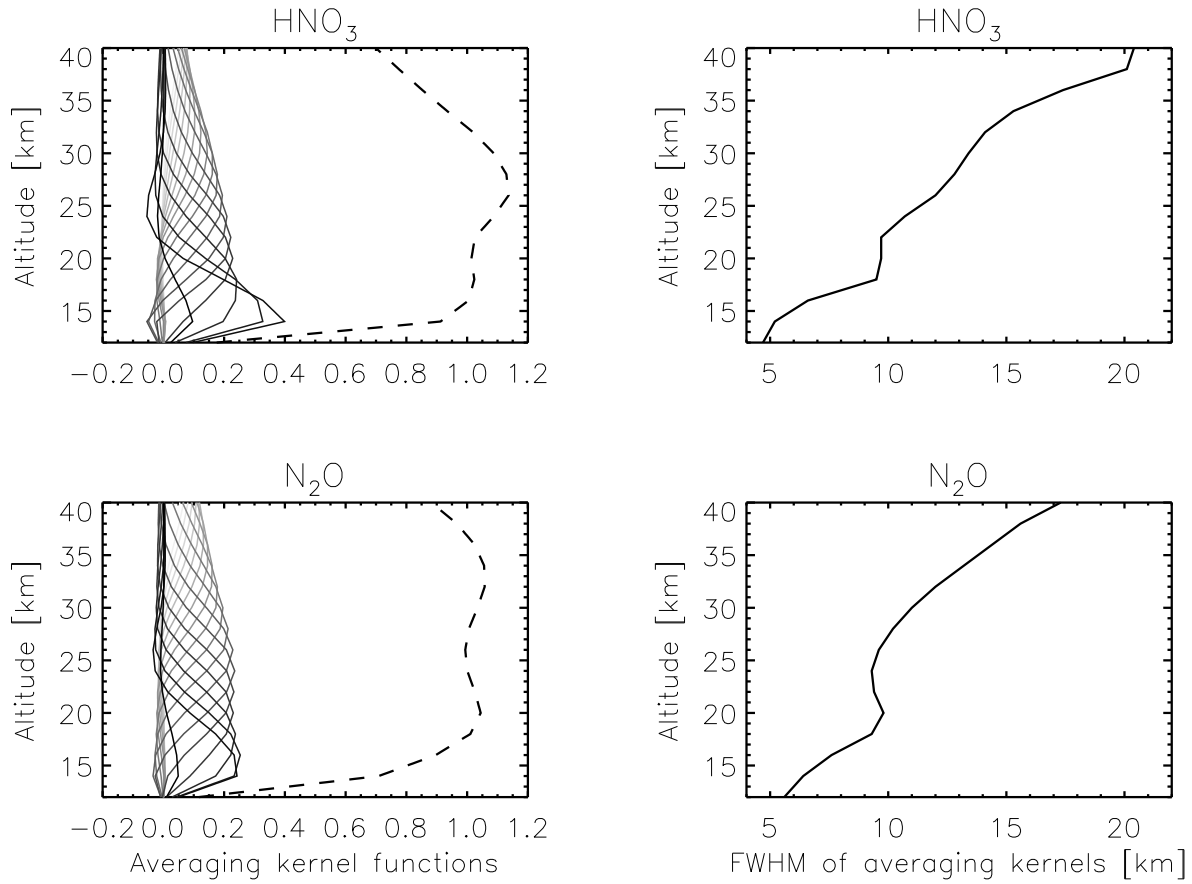

Figure 1. Averaging kernel functions (left) and the full width at half maximum of the averaging kernel functions (right) for a typical HNO_3 (upper part) and N_2O (lower part) measurement. The kernels at higher altitudes are drawn in successively lighter gray. The dashed line is the sum of the averaging kernels for a given retrieval altitude level.

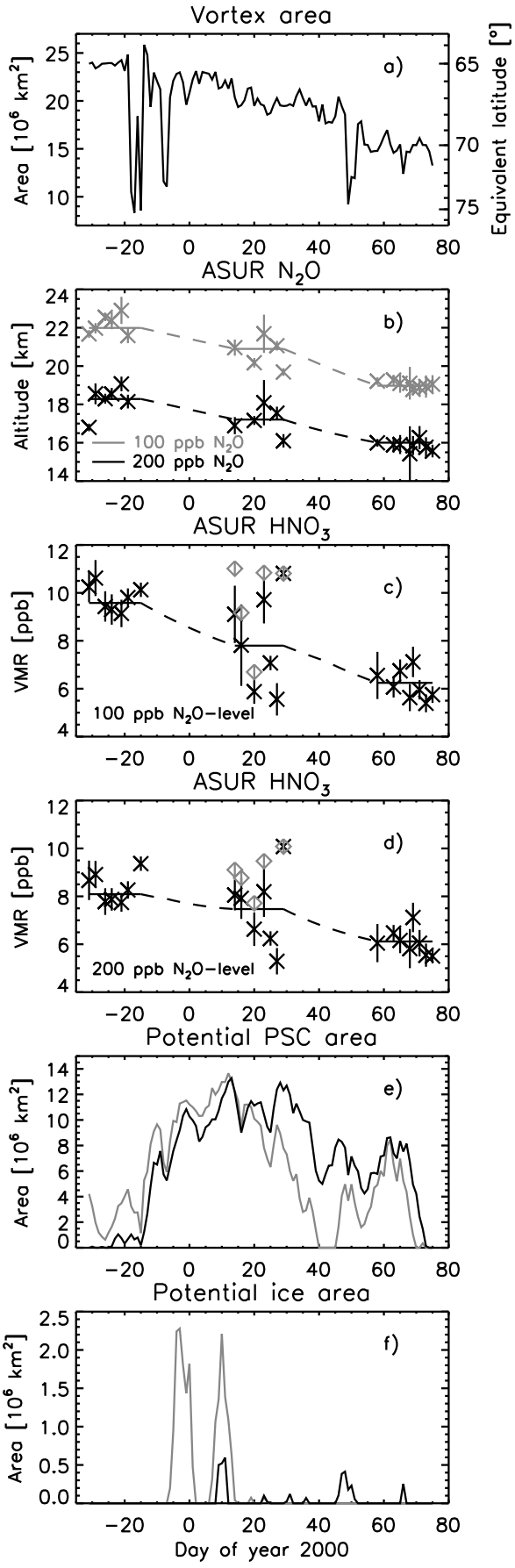
Vortex area
a)
Area [10^6 km^2]
Equivalent latitude [°]
ASUR N2O
b)
Altitude [km]
100 ppb N2O
200 ppb N2O
ASUR HNO3
c)
VMR [ppb]
100 ppb N2O−level
ASUR HNO3
d)
VMR [ppb]
200 ppb N2O−level
Potential PSC area
e)
Area [10^6 km^2]
Potential ice area
f)
Area [10^6 km^2]
Day of year 2000

Figure 2. a) Vortex area in winter 1999/2000. b) Altitude of 100 ppb N_2O-level (gray) and 200 ppb N_2O-level (black) measured by ASUR. The crosses show daily means inside the vortex, with the vertical bars giving the standard deviation. The solid horizontal lines show means over the campaigns, the dashed lines are interpolations in between. c) ASUR measurements of HNO_3 volume mixing ratios at 100 ppb N_2O. The crosses show again daily means, the vertical bars give the standard deviation, the horizontal bars show campaign means. The diamonds indicate means of measurements at positions without PSC coverage in January. d) ASUR measurements of HNO_3 volume mixing ratios at 200 ppb N_2O. The nomenclature of the symbols is similar to plot c). e) Potential PSC area calculated from ECMWF temperatures using a volume mixing ratio of 5 ppm H_2O and the HNO_3 from c) at 100 ppb N_2O (gray) and 200 ppb N_2O (black). f) Area below the frost point calculated from ECMWF temperatures using a volume mixing ratio of 5 ppm H_2O at 100 ppb N_2O (gray) and 200 ppb N_2O (black).

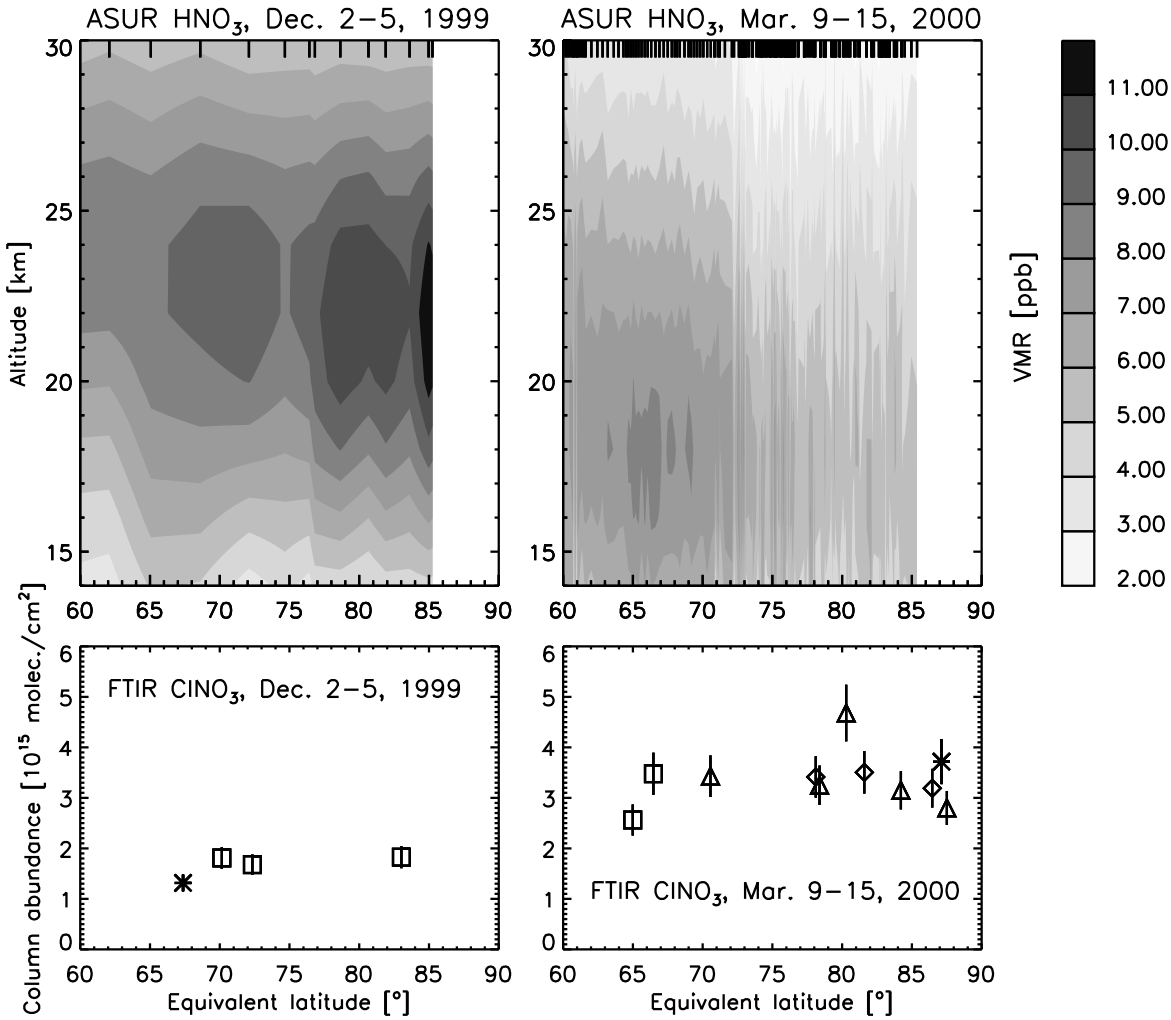

Figure 3. Upper part: HNO_3 volume mixing ratios measured by ASUR and plotted against equivalent latitude between December 2 and 5, 1999 (left) as well as between March 9 and 15, 2000 (right). The black vertical dashes on the top horizontal axis indicate where a measurement was made. Lower part: Vertical column abundances of $ClNO_3$ measured by different ground-based FTIR instruments and plotted against equivalent latitude for the same time spans as above. The rectangle stands for an FTIR measurement at Harestua, the triangle for a measurement at Kiruna, and the diamond for a ground-based measurement with the MkIV instrument at Esrange. The stars indicate the vertical columns derived from the profile measurements during the two balloon flights of the MkIV instrument. The vertical bars give the estimated accuracies.

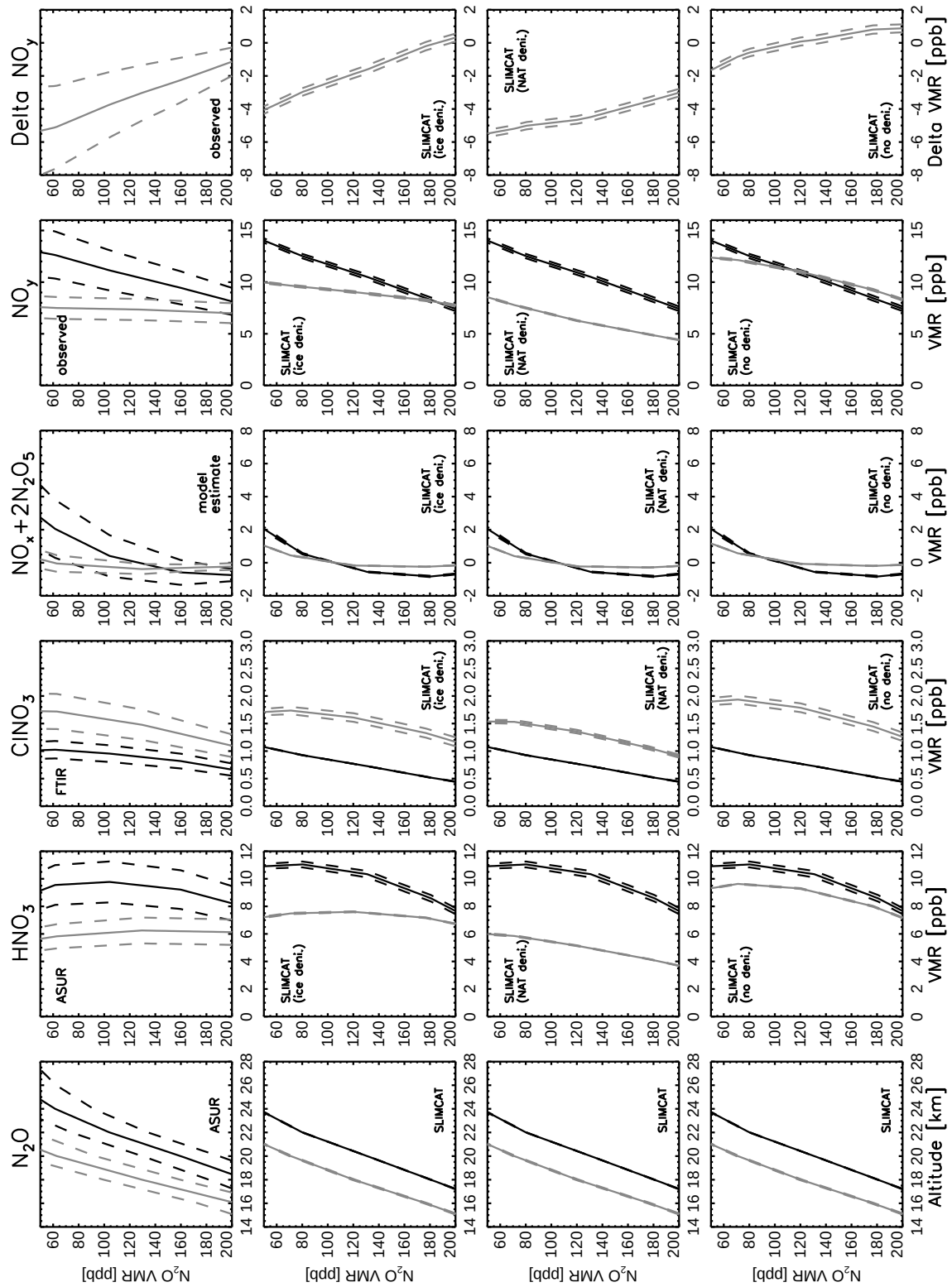
N2O
HNO3
ClNO3
NOx+2N2O5
NOy
Delta NOy
ASUR
FTIR
model estimate
observed
SLIMCAT (ice deni.)
SLIMCAT (NAT deni.)
SLIMCAT (no deni.)
SLIMCAT
N2O VMR [ppb]
Altitude [km]
VMR [ppb]
Delta VMR [ppb]

Figure 4. Vortex averaged profiles of N_2O, HNO_3, $ClNO_3$, $NO_x+2N_2O_5$, and NO_y as derived from measurements (top row), and modeled by the SLIMCAT model with ice denitrification (second row), with NAT denitrification (third row), and without denitrification (bottom row). The dashed lines show the full accuracy in the top row, and the standard deviation about the mean for the other rows. The black profiles show data between Dec. 2-5, 1999, the gray profiles show data between March, 9-15, 2000. The right column shows the denitrification as the difference between March and December NO_y after descending the December profiles according to the descent of the N_2O.

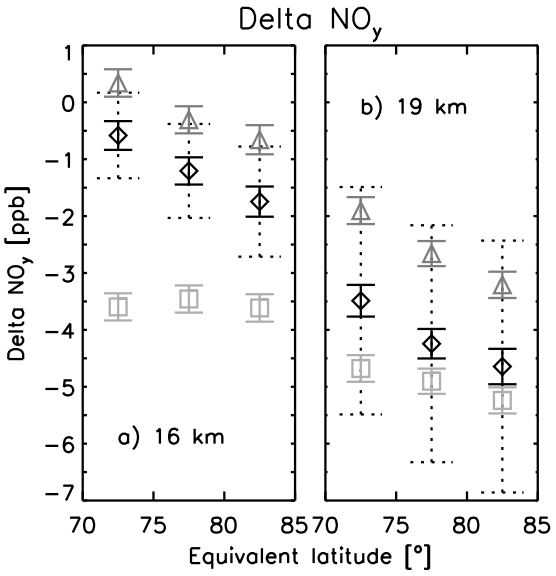

Figure 5. Average denitrification for regions between 85° and 80°, between 80° and 75° as well as between 75° equivalent latitude and the vortex edge for 16 km altitude (a) and for 19 km altitude (b) in mid-March. The diamonds show denitrification derived from measurements, with the solid error bars giving the standard deviation about the mean and the dotted error bars giving the full accuracy. The triangles show results from the SLIMCAT ice run, while the squares show results from the SLIMCAT NAT run, with the error bars giving the standard deviation about the mean in each case.